Spectrochimica Acta Part A: Molecular and Biomolecular Spectroscopy 123 (2014) 290–297

Contents lists available at ScienceDirect

Spectrochimica Acta Part A: Molecular and Biomolecular Spectroscopy

journal homepage: www.elsevier.com/locate/saa

DFT calculations of structure and vibrational properties of 2,2,2-trichloroethylacetate, $CH_3CO_2CH_2CCl_3$

Diego M. Gil, María E. Tuttolomondo, Aída Ben Altabef *,[1]

INQUINOA, CONICET, Instituto de Química Física, Facultad de Bioquímica, Química y Farmacia, Universidad Nacional de Tucumán, San Lorenzo 456, T4000CAN Tucumán, Argentina

HIGHLIGHTS

- The conformational behavior was studied by ab initio and DFT calculations.
- FTIR and Raman investigation of 2,2,2-trichloroethylacetate were carried out.
- The fundamental vibrational modes were assigned.
- NBO and AIM analysis were performed in order to investigate the conformational preference.

GRAPHICAL ABSTRACT

IR and Raman spectra of the liquid phase and both conformers for $CH_3CO_2CH_2CCl_3$.

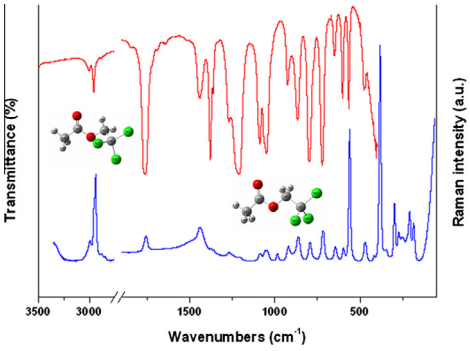

ARTICLE INFO

Article history:
Received 6 September 2013
Received in revised form 13 November 2013
Accepted 5 December 2013
Available online 17 December 2013

Keywords:
2,2,2-Trichloroethylacetate
Ab initio calculations
DFT calculations
Infrared and Raman spectroscopy

ABSTRACT

The molecular structure and conformational properties of 2,2,2-trichloroethylacetate, $CH_3CO_2CH_2CCl_3$, were determined by ab initio (MP2) and DFT quantum chemical calculations at different levels of theory. The theoretical study was complemented with experimental measurements such as IR and Raman spectroscopy. The experimental and calculations confirm the presence of two conformers, one with *anti, gauche* conformation (C_1 symmetry) and another with *anti, anti* form (C_s symmetry). The conformational preference was studied using the total energy scheme, NBO and AIM analysis. The infrared spectra of $CH_3CO_2CH_2CCl_3$ are reported in the liquid and solid phases and the Raman spectrum in liquid phase. Using calculated frequencies as a guide, evidence for both C_1 and C_s conformers is obtained in the IR and Raman spectra.

Introduction

The compound 2,2,2-trichloroethylacetate was first synthesized by Hill et al. through a Friedel–Craft reaction between acetic chloride and 2,2,2-trichloroethanol using as catalyst anhydrous aluminum chloride [1]. This compound is a convenient reactant for the acylation of different compounds. Theil et al. have reported the Pancreatin-Catalyzed acylation of *cis*-cyclopent-2-ene-1,4-diol with 2,2,2-trichloroethylacetate and they obtained a meso diacetate compound [2]. Other authors have reported the synthesis of different amines through intermolecular Rhodium-catalyzed C—H amination with 2,2,2-trichloroethyl-*N*-tosyloxycarbamate producing excellent yields [3,4].

The compound 2,2,2-trichloroethylacetate, $CH_3CO_2CH_2CCl_3$, is commercially available, but its molecular structure has not been studied. For $CH_3CO_2CH_2CCl_3$, infrared and Raman spectra have been recorded in liquid and solid phases. These experimental measurements were complemented by quantum chemical calculations to obtain an optimized molecular structure. Furthermore, the barrier to internal rotation around the O—CH_2 bond has been

* Corresponding author. Tel.: +54 381 4311044; fax: +54 381 4248169.
E-mail address: altabef@fbqf.unt.edu.ar (A. Ben Altabef).
[1] Member of the Carrera del Investigador Científico, CONICET, Argentina.

1386-1425/$ - see front matter © 2014 Published by Elsevier B.V.
http://dx.doi.org/10.1016/j.saa.2013.12.042

calculated using an assortment of computational approaches (*ab initio* and DFT) and fitted to a sixfold Fourier-type expansion. This methodology has allowed us to analyze the nature of the potential function and asses the preferred conformation of the molecule. The study was complemented by natural bond orbital (NBO) analysis to determine the presence of hyper-conjugative interactions, which would favor one conformation over another. We have compared the experimental and theoretical structures and conformations of $CH_3CO_2CH_2CCl_3$ with the experimental results obtained previously for different acetates with the general formula $CF_3C(O)OR$ (R = CH_3, CH_2CH_3 and CH_2CF_3) [5–7] and a thioacetate, $CF_3C(O)SCH_2CH_3$ [8].

Experimental

A sample of 2,2,2-trichloroethylacetate (Sigma–Aldrich) was used without further purification for both diffraction and spectroscopy measurements. All handling was performed under dry nitrogen to protect the sample from atmospheric humidity.

Infrared and Raman spectroscopy

Infrared spectra for $CH_3CO_2CH_2CCl_3$ in the liquid phase were recorded in the 4000–400 cm^{-1} range at room temperature (RT) using a Perkin–Elmer GX1 Fourier Transform infrared instrument. The spectrum of the substance in solid state was recorded after depositing it from the vacuum line onto a KBr window maintained at about −100 °C, in a variable-temperature RIIC (VLT-2) cell. The Raman spectrum of the liquid at RT between 3500 and 50 cm^{-1} were measured on a Thermoscientific DXR Smart Raman instrument. Data were collected using a diode-pump, solid state laser of 780 nm (5 cm^{-1} spectral resolution). A confocal aperture of 25 μm pinhole was used. In order to achieve a sufficient signal to noise, 100 expositions of 2 s were accumulated for the sample. The laser power was maintained at 5 mW when collecting data.

Computational details

Theoretical calculations were performed using the program package Gaussian 03 [9]. The potential energies associated with the C(1)O(3)C(4)C(5) and C(11)C(1)O(3)C(4) dihedral angles were calculated at MP2, B3LYP and mPW1PW91 levels using the 6-311++G(d,p) basis sets, with that torsional angle frozen and all other parameters allowed to relax. The total energy curves were prepared in steps of 10° using default convergence criteria as implemented in the Gaussian 03 program [9].

Geometry optimizations were performed at the MP2 [10] and DFT levels using a variety of basis sets. Electron correlation was then considered using the MP2 approach with the 6-31G(d), 6-311G(d,p) and 6-311++G(d,p) basis set [11–14]. DFT calculations were performed using Becke's three-parameter hybrid exchange functional [15] (B3) combined with both the Lee–Yang–Parr gradient-corrected correlation functional [16] (LYP) and the same basis sets as for the MP2 calculations. The second DFT method used, mPW1PW91 [17] applies a modified Perdew–Wang exchange functional and Perdew–Wang 91 correlation functional [17]. All calculations were performed using standard gradient techniques and default convergence criteria. The stability of the optimized geometries was confirmed by wavenumber calculations, which gave positive values for all the obtained wavenumbers. The vibrational modes were assigned by means of visual inspection using the Gaussview 05 program [18]. A comparison was performed between the theoretically calculated frequencies and the experimentally measured frequencies. In this investigation we observed that the calculated frequencies were slightly greater than the fundamental frequencies.

The prediction of Raman intensities was carried out by following the procedure outlined below. The Raman activities (S_i) were calculated by Gaussian 03 and converted to relative Raman intensity (I_i) using the following relation from the basic theory of Raman scattering [19]:

$$I_i = \frac{f(v_o - v_i)^4 S_i}{v_i[1 - \exp(-hcv_i/kT)]} \quad (1)$$

where v_o is the laser exciting wavenumber in cm^{-1} (in this work, we have used the excitation wavenumber v_o = 12,820.5 cm^{-1}, which corresponds to the wavelength of 780 nm of the solid state laser), v_i the vibrational wavenumber of the *i*th normal mode (in cm^{-1}), *h*, *c* and *k* are universal constants, and *f* is the suitably chosen common scaling factor for all the peaks intensities (10^{-12}).

A natural bond orbital (NBO) calculation was performed at the B3LYP/6-311++G(d,p) level using the program NBO 3.1 [20] as implemented in Gaussian 03 package. This analysis were performed in order to understand various second order interactions between the filled orbitals of one subsystem and vacant orbitals of another subsystem, with the aim of having a measure of the intra-molecular delocalization of hyper-conjugation. In addition, an analysis of the reactivity of the compound was done within Bader's atoms in molecules theory (AIM) by using the AIM2000 code [21,22].

Results and discussion

Quantum chemical calculations

Conformational stability

The potential energy surface scans for internal rotation around the C(1)—O(3)—C(4)—C(5) dihedral angle at the B3LYP, mPW1PW91 and MP2 levels using the 6-311++G(d,p) basis sets are shown in Fig. 1. There is a good agreement between the methods. The potential energy scans show two different minima, one with C_1 symmetry (*anti, gauche* conformation) and another with C_s symmetry (*anti, anti* conformation) as shown in Fig. 2, indicating that both conformers should exist because of the differences in total energy between the two minima are very small. Table S1 shows the absolute free energies of both conformers and the relative total energies and free energies calculated at the B3LYP and mPW1PW91 using the 6-311++G(d,p) basis sets. At the B3LYP/

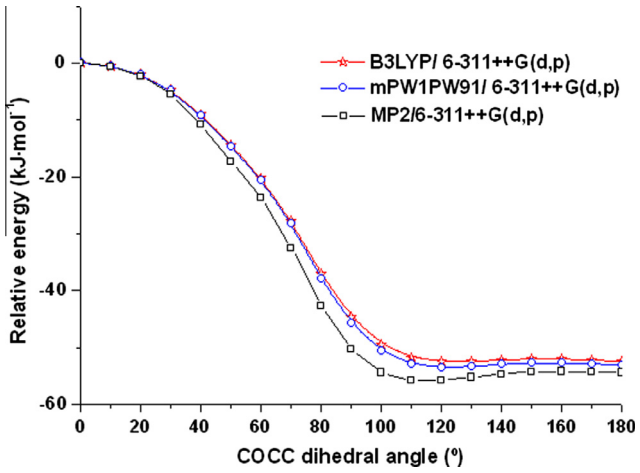

Fig. 1. Torsional potential around the O(3)—C(4) bond of $CH_3CO_2CH_2CCl_3$ calculated at B3LYP, mPW1PW91 and MP2 levels of theory using the 6-311++G(d,p) basis sets.

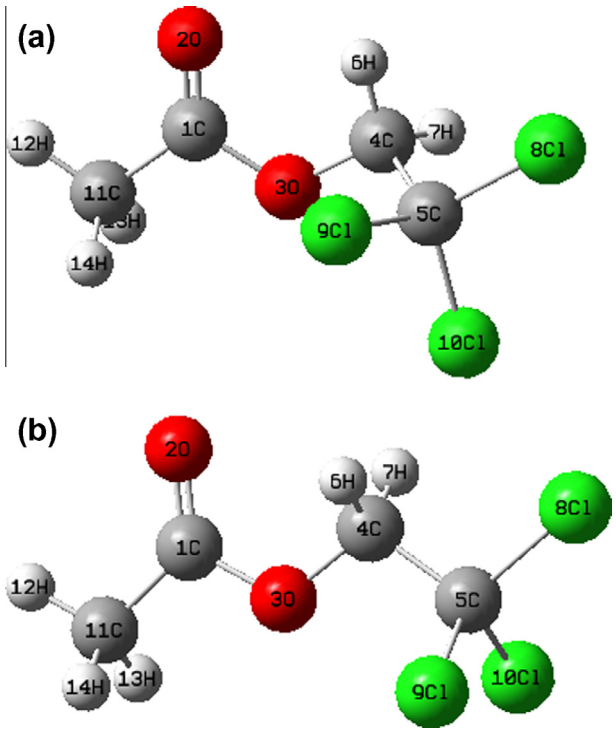

Fig. 2. Optimized molecular structures, including atoms numbering, of (a) *anti, gauche* (C_1) conformer and (b) *anti, anti* (C_s) conformer for $CH_3CO_2CH_2CCl_3$ calculated at the B3LYP/6-311++G(d,p) level.

6-311++G(d,p) level, the C_s symmetric conformer is lower in energy than the C_1 conformer by approximately 1.58 kJ mol^{-1}; at the mPW1PW91/6-311++G(d,p) level, the corresponding free energy difference was 2.46 kJ mol^{-1}. These results are in agreement with the calculations performed for related molecules in which the conformer with a mirror plane is predicted to be more stable [5–8]. All calculations showed that the CCl_3 groups in both conformers were staggered with respect to the CH_2 groups and the CH_3 groups were both oriented so that one C—H bond eclipsed the C=O bond (see Fig. 2).

For both conformers identified above, the free energies calculated using the B3LYP/6-311++G(d,p) level of theory were used, along with the average temperature of the experiment, to estimate (using the Boltzmann distribution) the amount of each conformer that should be observed in the gas phase. The difference in free energy was calculated to be 1.58 kJ mol^{-1}; therefore the ratio of C_1—C_s conformer was predicted to be 0.65:0.35.

Geometrical parameters

The optimized bond lengths, bond angles and dihedral angles for both conformers of $CH_3CO_2CH_2CCl_3$ are listed in Table 1. The experimental parameters in Table 1 are derived from gas electron diffraction (GED) measurements from $CF_3CO_2CH_2CF_3$ [6] and $CF_3CO_2CH_2CH_3$ [7]. As seen in Table 1, the bond lengths calculated at mPW1PW91/6-311++G(d,p) level for both conformers are in agreement with the experimental data, although large differences are observed with respect to the C=O and O(3)—C(4) bonds. The B3LYP method reproduces better these bonds. The predicted C(1)=O(2) bond lengths for C_1 and C_s conformers are 1.202 and 1.204 Å, respectively, calculated at the B3LYP/6-311++G(d,p) level. These values are closer to those 1.212 and 1.213 Å obtained through GED measurements for $CF_3CO_2CH_2CF_3$ [6] and $CF_3CO_2CH_2CH_3$ [7], respectively. A comparison between the calculated and the experimental bond angles in $CF_3CO_2CH_2CF_3$ and $CF_3CO_2CH_2CH_3$ show a good correlation.

NBO analysis

NBO analysis has frequently been used in the investigation of the anomeric effect and the origin of the internal rotation barrier. NBO analysis allows us to estimate the energy of the molecule with the same geometry but in the absence of the electronic delocalization. Moreover, only the steric and electrostatic interactions through the term E_{Lewis} are taken into account. The energy barrier $\Delta E_{Barrier}$ could be written as a function of bond strength, hyperconjugative and steric repulsions:

$$\Delta E_{Barrier} = \Delta E_{Lewis} + \Delta E_{deloc.} = \Delta E_{Struct.} + \Delta E_{exc.} + \Delta E_{deloc.} \quad (2)$$

where $\Delta E_{Struct.}$ takes into account Coulomb and bond energy changes in the classical structure, ΔE_{exc} (known as the Pauli exchange or steric repulsion energy) accounts for the non-Coulombic energy changes arising from the Pauli exclusion principle, and ΔE_{deloc} describes the hyperconjugative stabilization.

Table 2 shows the contribution from the localized electron density (E_{Lewis}) and the delocalized electron density (E_{deloc}) to the rotation barrier around the O(3)—C(4) bond at the B3LYP/6-311++G(d,p) level of theory. The relative total energies of the

Table 1
Optimized geometrical parameters (bond lengths, bond angles and selected dihedral angles) for both conformers of $CH_3CO_2CH_2CCl_3$ calculated with different levels of theory.

Parameter[a]	C_1 conformer			C_s conformer			Experimental
	B3LYP 6-311++G(d,p)	mPW1PW91 6-311++G(d,p)	MP2 6-311++G(d,p)	B3LYP 6-311++G(d,p)	mPW1PW91 6-311++G(d,p)	MP2 6-311++G(d,p)	
C(11)—H (mean)	1.091	1.090	1.091	1.091	1.090	1.091	1.081[b]
C(1)—C(11)	1.052	1.495	1.502	1.503	1.496	1.503	1.546
C(1)=O(2)	1.202	1.198	1.206	1.204	1.199	1.210	1.213[b]
C(1)—O(3)	1.371	1.361	1.373	1.362	1.353	1.362	1.330[b]
O(3)—C(4)	1.422	1.412	1.417	1.425	1.414	1.422	1.456[b]
C(4)—C(5)	1.531	1.524	1.525	1.526	1.520	1.520	1.512[b]
C(5)—X (F, Cl)	1.798	1.779	1.773	1.797	1.779	1.773	–
C(11)—C(1)—O(3)	110.1	110.1	109.3	110.7	110.7	110.1	106.9[b]
O(2)=C(1)—O(3)	123.5	123.5	123.9	122.7	122.6	122.8	123.2[c]
C(1)—O(3)—C(4)	117.7	117.4	116.5	115.7	115.3	113.9	114.6[b]
O(3)—C(4)—C(5)	110.2	110.2	109.5	108.4	108.4	107.4	109.3[b]
Cl—C(5)—Cl	109.5	109.7	110.2	109.5	109.7	110.0	–
C11—C1—O3—C4	177.3	176.8	174.2	180.0	180.0	180.0	–
C1—O3—C4—C5	123.2	121.1	114.0	180.0	180.0	180.0	–

[a] Bond lengths in Å, angles in degrees. See Fig. 2 for atoms numbering.
[b] Taken from Ref. [7].
[c] Taken from Ref. [6].

Table 2
Contribution of Lewis energy (E_{Lewis}) due to the localized electron density and the hyperconjugation energy (E_{deloc}) due to the delocalized electron density to barrier for C_s and C_1 conformers and the transition state (TS) rotamer of $CH_3CO_2CH_2CCl_3$ at the B3LYP/6-311++G(d,p) level.

Structure	E_{Lewis} (Hartrees)	ΔE_{Lewis} (kJ mol^{-1})	E_{deloc} (Hartrees)	ΔE_{deloc} (kJ mol^{-1})
anti, anti (C_s)	−1685.927114059	−104.61	−0.722255	52.22
TS	−1685.887230494	0	−0.742163	0
anti, gauche (C_1)	−1685.923613653	−95.43	−0.725801	42.92

various conformers as well as the Lewis and delocalization energy contributions to the relative energies upon rotation are presented in Fig. S1. Table 2 indicates that the Lewis energy is critical for the determination of the energetic preference; its minimum corresponds to the *anti, anti* conformer with C_s symmetry (see Fig. S1). The delocalization energy difference, $\Delta E_{deloc,}$ for the *anti, anti* conformer is greater than *anti, gauche* conformer indicating that ΔE_{deloc} favors the *anti, gauche* conformation. Similar results were obtained by Defonsi Lestard et al. in different trifluoroacetates [5–8].

Table 3 shows the most relevant hyperconjugative interactions at the B3LYP/6-311++G(d,p) level resulting from NBO calculations for both conformers of $CH_3CO_2CH_2CCl_3$. According to the NBO analysis, the hypercopnjugative interactions are more favored in the C_s conformer than in C_1 conformer. As seen in Table 3, the hyperconjugative effect LP O(3) → σ* C(4)—C(5) is higher in the *anti, gauche* conformer than *anti, anti* one, indicating that this interaction is very important for the stabilization of the *anti, gauche* conformation. The anomeric orbital interaction LP O(3) → σ* C(1)—C(11), only appears in the *anti, gauche* conformer with an energy value of 2.3 kJ mol^{-1}. Similar results were obtained in different acetates such as $CF_3CO_2CH_2CF_3$ [6] and $CF_3CO_2CH_2CH_3$ [7].

The relation between the electron occupation of the σ* C(4)—O(3), σ* C(4)—C(5) and σ* C(1)—O(2) and the bond lengths C—O, C—C and C=O has been investigated in both conformers. Table S2 shows the C—O, C—C and C=O bond lengths with the corresponding electron occupancy of the natural bond orbitals for both conformers of $CH_3CO_2CH_2CCl_3$. As shown in Table S2, the C(4)—O(3) bond length in C_s conformer is longer than that of C_1 conformer, which is in agreement with the high occupation of the σ* C(4)—O(3) orbital in C_S conformer compared with C_1 conformer. These results are in agreement with the high value of energy of LP O(3) → σ* C(4)—C(5) interaction in C_1 conformer (see Table 3) which produce a lengthening of the C(4)—C(5) bond length and a shortening of the C(4)—O(3) bond length. The energy interaction LP O(3) → σ* C=O is higher in $CF_3CO_2CH_2CF_3$ [7] compared with the same energy interaction in $CH_3CO_2CH_2CCl_3$. The greater anomeric effect observed in $CF_3CO_2CH_2CF_3$ produces a shortening of the C—O bond distance and a lengthening of the C=O bond distance compared with those reported in Table 1 for $CH_3CO_2CH_2CCl_3$.

Table 3
Important hyperconjugative interactions in kJ mol^{-1} for C_1 and C_S conformers of $CH_3CO_2CH_2CCl_3$ calculated at the B3LYP/6-311++G(d,p) level.

Interaction[a]	*Anti, gauche* (C_1)	*Anti, anti* (C_s)
LP O(2) → σ* C(1)—C(11)	82.72	83.18
LP O(2) → σ* C(1)—O(3)	152.82	149.56
LP O(3) → σ* C(1)—O(2)	200.97	205.61
LP O(3) → σ* C(4)—C(5)	18.09	5.43
LP O(3) → σ* C(1)—C(11)	2.13	–
LP O(3) → σ* C(4)—H(6)	12.08	24.33
LP O(3) → σ* C(4)—H(7)	21.99	24.33
LP Cl(8) → σ* C(4)—C(5)	16.47	16.22
LP Cl(9) → σ* C(4)—C(5)	19.06	19.65
LP Cl(10) → σ* C(4)—C(5)	19.48	19.65
Total	545.81	547.96

[a] LP indicates electron lone pair on the specified atom (See Fig. 2 for atoms numbering).

Internal barrier decomposition schemes

The study of the nature of the internal rotation barrier around the O—C bond, in terms of hyper-conjugative, steric and electrostatic interactions, gives information about the stability of the different conformations. The total energy surface for this torsion angle was calculated in the range of 0–180° in steps of 10°, relaxing all geometrical parameters except the one to be scanned. The energy profiles were fitted to a sixth-order Fourier expansion:

$$V(\theta) = \sum_{i=1}^{6} \frac{1}{2} V_{iN}(1 - \cos iN\theta) \quad (3)$$

where N is the symmetry number and it is 1. No contributions of zero-point energy were taken into account.

Decomposition of the total energy function and the analysis of the different V_i terms have previously described as a simple way to analyze the stabilization of different conformations in molecular systems [5–8]. Fig. S2 shows the Fourier decomposition of the total energy function calculated at B3LYP/6-311++G(d,p) level of theory. The terms V_1 and V_2 are the main contributions to the rotation barrier, where $V_1 > V_2 > V_3 > V_4$. The terms V_5 and V_6 are less significant when deconvoluting the potential-energy curve. V_2 is associated with conjugative and hyper-conjugative effects that have a periodicity of 180°. In this case V_2 is large and positive, indicating that the contribution of the hyper-conjugative effect stabilizes the *anti, anti* conformation of $CH_3CO_2CH_2CCl_3$. V_1 generally accounts the interactions between local dipoles and for steric interactions (electrostatic effect); this value is large and positive indicating that there is a strong preference for the *anti, anti* conformation over the *anti, gauche* one (see Table S3). In order to confirm the contributions of the different terms in the Fourier decomposition, we have performed an investigation of the energy barrier based on the partition offered by the scheme:

$$\Delta E = \Delta E_{nn} + \Delta E_{en} + \Delta E_{ee} + \Delta E_K \quad (4)$$

where ΔE is the total energy change between structures of different geometries, ΔE_{nn} is the energy change for the nuclear repulsions, ΔE_{en} is the change in electronic-nuclear attraction energy, ΔE_{ee} is the change in electron repulsions, and ΔE_K is the change in kinetic energy. It can be seen that Eq. (4) describes the total energy change as a sum of all potential and kinetic contributions.

The results for the energy as function of the COCC dihedral angle are shown in Fig. S3. This figure illustrates the fact that the repulsive terms, ΔE_{ee} and ΔE_{nn} are smaller in the C_s conformer compared with the C_1 one, while the attractive terms, ΔE_{en} favor the *anti, gauche* conformation with C_1 symmetry.

The relative stabilization of the C_s conformer could be interpreted as a repulsive interaction between the lone pairs on the O(3) and the electronic charge of the C(4)—C(5) bond, which is minimized when the symmetry is C_s. This is in agreement with the behavior of the repulsive terms ΔE_{ee} and ΔE_{nn} that are smaller in the C_s conformer.

AIM analysis

The quantum theory of atoms in molecules has been useful in the characterization of bonds through a topological analysis of the electronic charge density and their Laplacian at the Bond Critical Points (BCP) [21]. In the AIM theory the nature of the bonding interaction can be determined through an analysis of the properties of the charge density ρ, and its Laplacian $\nabla^2(\rho)$ at the BCP, and through the properties of the atoms, which are obtained by integrating the charge density over the atom orbitals [21]. Table 4 shows the bond critical point data for both conformers of CH_3CO_2-

CH_2CCl_3. As seen in Table 4, the value of the charge density at the C(1)—O(3) bond critical point is relatively high for both conformers and the Laplacian of electron density is negative hence indicating that the charge density has been concentrated in the inter-nuclear region. Besides, the value of charge density of the C—O bond in C_s conformer is greater than C_1 conformer, which leads to a decrease in the C—O bond length. The value of charge density at the C(1)═O(2) bond critical point in C_1 conformer is slightly greater than C_s conformer and the Laplacian of charge density of both conformers are negative. In this case, the C═O bond length in C_s conformer is slightly greater than C_1 one. These results are in agreement with NBO analysis (see Table 3) which shows that LP O(3) → σ* C(1)═O(2) interaction is more important in the *anti, anti* conformation (C_s symmetry). This effect produces a lengthening of the C(1)═O(2) bond and a shortening of the O(3)—C(1) bond as compared with that of *anti, gauche* (C_1) conformer.

Vibrational analysis

The assignment of the experimental infrared absorption and Raman dispersion bands to the normal modes of vibration of $CH_3CO_2CH_2CCl_3$ was based on the comparison of related molecules [6–8,23–26] and assisted by the theoretical calculations performed in this work with B3LYP/6-311++G(d,p) level of theory.

The FTIR and Raman spectra of the liquid are shown in Fig. 3. Fig. 4 illustrates the FTIR spectra of the liquid and solid substance. The simulated IR and Raman spectra of both conformers of the title compound are shown in Figs. S4 and S5, respectively. The wavenumbers of the observed spectral and the approximate descriptions of the modes of both conformers of $CH_3CO_2CH_2CCl_3$ are given in Table 5. Infrared and Raman spectroscopy are important techniques for quantitative conformational analysis. The C_1 conformer is 1.58 kJ mol^{-1} higher in free energy at the B3LYP/6-311++G(d,p) method than the C_s conformer and at room temperature, C_1 and C_s can be expected to be significantly populated. The conformationally averaged IR and Raman spectra are obtained by summing the population-weighted spectra of C_1 and C_s conformers calculated by using B3LYP/6-311++G(d,p) frequencies and intensities considering Lorentzian band shapes (γ = 2 cm^{-1}). The population are calculated from the B3LYP/6-311++G(d,p) energy difference via Boltzmann statistics and amount to 65% and 35%, respectively.

Table 4
The B3LYP/6-311++G(d,p) calculated Bond Critical Point (BCP) data and BCP distances (in a.u.) to attractors.

	C_1 conformer	C_s conformer
C(1)—O(3)		
ρ	0.2838	0.2884
$\nabla^2(\rho)$	−0.4972	−0.4596
BCP—C(1)	0.9069	0.8925
BCP—O(3)	1.6853	1.6836
d (Å)	1.371	1.362
q C(1)	0.1610	0.2511
q O(3)	0.0225	0.0182
v (cm^{-1})	1221	1241
C(1)═O(2)		
ρ	0.4222	0.4206
$\nabla^2(\rho)$	−0.1492	−0.1688
BCP—C(1)	0.7771	0.7788
BCP—O(2)	1.4938	1.4963
d (Å)	1.202	1.204
q C(1)	0.1610	0.2511
q O(2)	−0.2622	−0.2686
v (cm^{-1})	1817	1806
O(3)—C(4)		
ρ	0.2496	0.2495
$\nabla^2(\rho)$	−0.4016	−0.4268
BCP—O(3)	1.7529	1.7523
BCP—C(4)	0.9366	0.9423
d (Å)	1.422	1.425
q O(3)	0.0225	0.0182
q C(4)	−0.7359	−0.9385
v (cm^{-1})	1096	1104

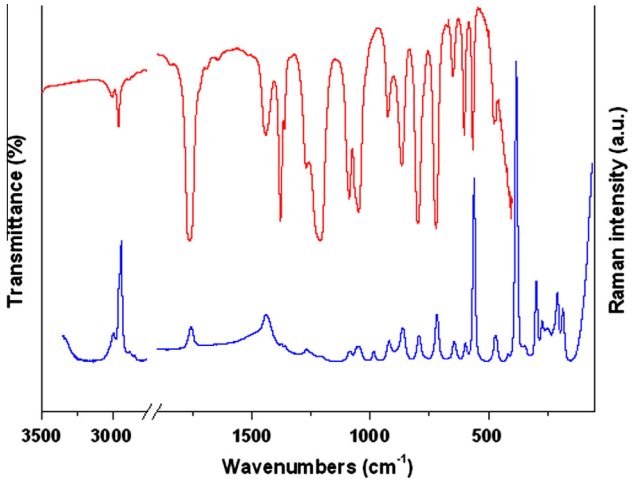

Fig. 3. Infrared and Raman spectra of the liquid phase of $CH_3CO_2CH_2CCl_3$.

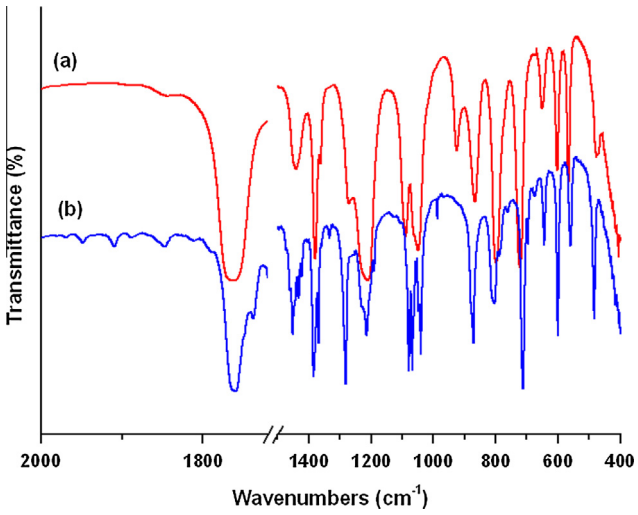

Fig. 4. Infrared spectra of $CH_3CO_2CH_2CCl_3$: (a) Liquid phase and (b) Solid phase.

At room temperature, most of the bands are attributable to the same fundamental for both conformations. The IR (liquid and solid) and Raman spectra demonstrated the presence of C_1 and C_s conformers by the resolution of several fundamental modes of vibration. The profiles of both conformers have been simulated in Figs. S4 and S5. The predicted conformational splittings for the modes are in good agreement with the observed splitting in the IR spectrum of the solid substance.

Assignment of bands

Methyl and methylene group modes

In the IR spectrum of the liquid, two bands appear in the C—H stretching region located at 3022 and 2882 cm^{-1}, which can be assigned to the CH_3 anti-symmetric and symmetric stretching modes, respectively. Typical shapes and intensities of the CH_3 group are observed in the Raman spectrum of the liquid, and the

Table 5
Observed and calculated wavenumbers (in cm^{-1}) and tentative assignments for the C_1 and C_s conformers of $CH_3CO_2CH_2CCl_3$.

Mode	Experimental			Calculated (B3LYP/6-311++G(d,p)		Approximate description of mode[c]
	IR (liquid)[a]	IR (−100 °C)	Raman (liquid)[b]	C_1 conformer	C_s conformer	
1	3022 sh	3017 m	3022 (5)	3160	3160	ν_a CH_3
2	3003 w (C_1) 2956 m (C_s)	3008 sh 2968 w	2996 (9)	3140	3130	ν_a CH_2
3	–	–	–	3113	3113	ν_a CH_3
4	–	2943 w	2938 (40)	3078	3073	ν_s CH_2
5	2882 vw	2885 vw	2880 (3)	3053	3053	ν_s CH_3
6	1763 vs	1761 vs (C_1) 1748 sh (C_s)	1763 (10) 1756 (11)	1817	1806	ν C=O
7	1450 sh (C_s) 1443 m (C_1)	1460 w 1452 m	1446 (15)	1481	1486	δ CH_2
8	1436 sh	1433 w	1438(15)	1475	1475	δ_a CH_3
9	1427 sh	1422 w	1427 sh	1471	1471	δ_a CH_3
10	1380 s	1385 s	1377 (6)	1408	1410	δ_s CH_3
11	1362 w	1368 w	1358 (5)	1394	1394	ω CH_2
12	1273 m	1281 m (C_1) 1255 vw (C_s)	1268 (4) 1246 (3)	1302	1275	$\tau\omega$ CH_2
13	1224 sh (C_s) 1211 m (C_1)	1229 sh 1214 m	1212 (5)	1221	1242	ν C(1)—O(3)
14	1088 m	1080 m	1085 (3)	1096	1104	ν C(4)—O(3)
15	1062 sh (C_1) 1050 s (C_s)	1067 m 1055 w	1060 (5) 1055 (5)	1080	1068	ρ CH_3
16	1046 sh	1047 w	1047 (5)	1066	1066	ρ CH_3
17	-	1040 sh	-			ρ CH_2
18	-	987 w	985 (3)	994	990	ν C(4)—C(5)
19	925 vw (C_s) 867 w (C_1)	928 w 870 w	920 (2) 863 (11)	880	941	ν C(1)—C(11)
20	799 m	802 m (C_1) 789 w (C_s)	795 (8)	770	763	ν_a CCl_3
21	722 m	715 m (C_1) 697 vvw (C_s)	717 (15)	693	691	ν_a CCl_3
22	652 vw	653 sh (C_s) 645 vw (C_1)	645 (6)	647	658	δ in plane C=O
23	603 w	601 w	598 (6)	601	601	δ out of plane C=O
24	567 w	565 w	561 (62)	558	555	ν_s CCl_3
25	494 sh (C_1) 476 vw (C_s)	498 sh 483 vw	472 (9)	474	458	δ C(11)—C(1)—O(3)
26	–	–	382 (100)	384	379	δ_s CCl_3
27	–	–	345 (5)	352	347	δ_a CCl_3
28	–	–	298 (27)	299	299	δ_a CCl_3
29	–	–	272 (13)	276	257	δ C(1)—O(3)—C(4)
30	–	–	247 (10) (C_1) 222 (2) (C_s)	244	224	δ O(3)—C(4)—C(5)
31	–	–	208 (22)	209	207	ρ CCl_3
32	–	–	185 (17)	186	183	ρ CCl_3
33	–	–	–	87	99	τ C(1)—O(3)
34	–	–	–	64	69	τ CH_3
35	–	–	–	49	44	τ CCl_3
36	–	–	–	34	21	τ C(4)—O(3)

[a] sh, Shoulder; s, strong; w, weak; m, medium; v, very.
[b] Relative band heights in parentheses.
[c] ν, Stretching; δ, bending; ρ, rocking; ω, wagging; $\tau\omega$, twisting; τ; torsion.

bands located at 3022 and 2880 cm^{-1} are attributed to the same modes of vibration.

The shoulders located at 1436 and 1427 cm^{-1} in the IR spectrum of the liquid are assigned to the CH_3 anti-symmetric deformation. The IR spectrum of the solid substance shows two weak bands at 1433 and 1422 cm^{-1} assigned to the modes mentioned previously. The corresponding CH_3 symmetric deformation is assigned to the band located at 1380 cm^{-1} in the IR spectrum of the liquid (1377 cm^{-1} in Raman). The bands corresponding to the CH_3 rocking mode appear split in the IR and Raman spectra indicating the presence of the two conformations mentioned above.

The bands located at 3003 and 2956 cm^{-1} in the IR spectrum of the liquid are assigned to the CH_2 anti-symmetric stretching mode for C_1 and C_s conformers, respectively. These bands appear at 2996 and 2952 cm^{-1} in the Raman spectrum. The band corresponding to the CH_2 symmetric stretching mode appear in the IR spectrum of the solid as a weak band located at 2943 cm^{-1} and as a medium intensity band at 2938 cm^{-1} in the Raman spectrum.

The bands located at 1450 and 1443 cm^{-1} in the IR spectrum are assigned to the CH_2 bending mode of C_s and C_1 conformers, respectively. The band located at 1446 cm^{-1} in the Raman spectrum could be assigned to the same mode. The location of these bands is in good correlation with related compounds. This mode is observed in $CF_3CO_2CH_2CF_3$ [6] at 1454 cm^{-1} and in $CF_3CO_2CH_2$-CH_3 [7] at 1478 cm^{-1}. The vibrations of CH_2 group as a structural unit appear in the IR spectrum of the liquid at 1362 cm^{-1} (wagging), 1273 cm^{-1} (twisting) and 1040 cm^{-1} (rocking). The Raman spectrum of the liquid shows two bands at 1268 and 1246 cm^{-1} indicating the presence of both conformers in the liquid. The same splitting of the band corresponding to the twisting mode of CH_2 was observed in the IR spectrum of the solid substance. All these observations are in agreement with quantum chemical calculations.

Carbonyl group modes

In the IR spectrum of the solid, the strong band at 1761 cm^{-1} and a shoulder located at 1748 cm^{-1} are assigned to the C=O stretching mode. The first band corresponds to the C_1 conformer and the second is assigned to the C_s conformer. These bands are in agreement with the values predicted by calculations performed at B3LYP/6-311++G(d,p). For the *anti, gauche* conformer this mode appears at 1817 cm^{-1} and for the *anti, anti* conformer the value calculated is 1806 cm^{-1}.

The experimentally observed frequency shift $\Delta\nu$(C=O) in the IR spectrum of the solid is 13 cm^{-1} and the B3LYP/6-311++G(d,p) method predicts a value of 11 cm^{-1} for the difference between *anti, gauche* and *anti, anti* conformations. Therefore, the comparison of experimental and calculated $\Delta\nu$(C=O) frequency shift confirms the assignment of the stronger band at 1761 cm^{-1} to the *anti, gauche* form and the weaker band at 1748 cm^{-1} to the *anti, anti* conformer.

The shoulder and a weak band observed at 653 and 645 cm^{-1} in the IR spectrum of the solid are assigned to the C=O in-plane bending mode, which could be assigned to the modes corresponding to

C_s and C_1 conformers, respectively. The weak band located at 603 cm^{-1} in the IR spectrum of the liquid is assigned to the C=O out of plane bending mode.

Trichloromethyl group modes

The assignment of the bands corresponding to the CCl_3 group was made by comparison with related molecules [25–29] and with quantum chemical calculations.

The two medium intensity absorption bands observed at 799 and 722 cm^{-1} in the IR spectrum (795 and 717 cm^{-1} in Raman) are assigned to the CCl_3 antisymmetric stretching modes. Both bands appear split indicating the presence of both cionformations. In $CCl_3SOC(O)CH_3$ [29], these bands appear at 766 and 738 cm^{-1}. The strongest band in the Raman spectrum of the liquid, at 382 cm^{-1} is assigned to the CCl_3 symmetric deformation, which is theoretically predicted at 384 and 379 cm^{-1} for C_1 and C_s conformers, respectively.

According to the theoretical calculations, the CCl_3 symmetric stretching mode is assigned to the band located at 567 cm^{-1} in the IR spectrum of the liquid. The IR spectrum of the solid shows a weak band at 565 cm^{-1} and an intense band located at 561 cm^{-1} in the Raman spectrum. For $CCl_3CH_2OSO_2NH_2$, this mode appears as a band located at 616 cm^{-1} [26].

The two bands observed in the Raman spectrum at 345 and 298 cm^{-1} are assigned to the CCl_3 antisymmetric deformation. The bands corresponding to the rocking of CCl_3 are observed in the Raman spectrum at 208 and 185 cm^{-1}. These bands appear at 225 and 187 cm^{-1} in the Raman spectrum of $CCl_3SOC(O)CH_3$ [29].

Skeletal modes

The band corresponding to the C(1)—O(3) stretching mode appears split into two components at 1224 and 1211 cm^{-1} in the IR spectra of the liquid and the solid, again indicating the presence of the two conformers. The medium intensity band located at 1088 cm^{-1} in the IR spectrum of the liquid (1085 cm^{-1} in the Raman spectrum) is assigned to the C(4)—O(3) stretching mode. The weak band observed in the IR spectrum of the solid at 987 cm^{-1} is assigned to the C(4)—C(5) stretching mode and the bands observed at 925 and 867 cm^{-1} in the IR spectrum of the liquid are assigned to the C(1)—C(11) stretching mode for C_s and C_1 conformers, respectively. This assignment was in agreement with calculations.

The shoulder located at 494 cm^{-1} and the weak band at 476 cm^{-1} are assigned to the CCO bending mode of C_1 and C_s conformers, respectively, and the band located at 272 cm^{-1} in the Raman of the liquid is assigned to the COC bending mode. The band corresponding to the OCC bending mode is observed split in the Raman spectrum at 247 and 222 cm^{-1}, the first one corresponds to the C_1 conformer and the second one to the C_s conformer.

Torsional modes

The bands corresponding to the torsional modes have not been observed in the Raman spectrum of the liquid.

Conclusions

The optimized molecular geometries and the conformational evaluation for $CH_3CO_2CH_2CCl_3$ have been calculated using MP2 and DFT techniques and different basis sets. The structural results indicate that the *anti, anti* conformation (C_s symmetry) is the most stable form. The decomposition of the potential-energy function as a Fourier expansion and the analysis of the different terms (V_i) have been useful to analyze the relative stabilities of different conformations of this molecular system. In this case V_2 is large and positive, indicating that the contribution of the hyper-conjugative effect stabilizes the *anti, anti* conformation (C_s symmetry). V_1 generally accounts the interactions between local dipoles and for steric interactions (electrostatic effect); this value is large and positive indicating that there is a strong preference for the *anti, anti* conformation over the *anti, gauche* one.

The NBO analysis has been performed in order to justify the preferred conformation of $CH_3CO_2CH_2CCl_3$. We conclude that the electrostatic and steric contributions included in the Lewis term tend to promote the *anti, anti* conformer, whereas the delocalization contribution tends to favor the *anti, gauche* conformer, as expected from the anomeric effect. The hyper-conjugative interactions are more favored in the C_s conformer than in C_1 one. These results were confirmed by AIM analysis.

The analysis of the IR (liquid and solid phases) and the Raman spectra of $CH_3CO_2CH_2CCl_3$ agrees with the presence of C_1 and C_s conformers and we have assigned 32 out the expected 36 normal modes of vibration. Two bands are clearly identified in the carbonyl stretching region in the IR spectrum of the solid substance measured at low temperature; the very strong band located at 1761 cm^{-1} can be assigned to the C_1 conformer and the shoulder at 1748 cm^{-1} indicates the presence of the C_s conformer.

Acknowledgments

D.M.G., M.E.T. and A.B.A. thank CIUNT and CONICET (PIP 0629) for financial support. D.M.G. thanks CONICET for a postdoctoral fellowship.

Appendix A. Supplementary material

Supplementary data associated with this article can be found, in the online version, at http://dx.doi.org/10.1016/j.saa.2013.12.042.

References

[1] M.E. Hill, J. Am. Chem. Soc. 75 (1953) 3020.
[2] F. Theil, H. Schick, M.A. Lapitskaya, K.K. Pivnitsky, Liebigs Ann. Chem. (1991) 195.
[3] H. Lebel, K. Huard, Org. Lett. 9 (2007) 639.
[4] K. Huard, H. Lebel, Chem. Eur. J. 14 (2008) 6222.
[5] M.E. Defonsi Lestard, M.E. Tuttolomondo, D.A. Wann, H.E. Robertson, D.W.H. Rankin, A. Ben Altabef, J. Raman Spectrosc. 41 (2010) 1357.
[6] M.E. Defonsi Lestard, M.E. Tuttolomondo, E.L. Varetti, D.A. Wann, H.E. Robertson, D.W.H. Rankin, A. Ben Altabef, J. Mol. Struct. 917 (2009) 183.
[7] M.E. Defonsi Lestard, M.E. Tuttolomondo, E.L. Varetti, D.A. Wann, H.E. Robertson, D.W.H. Rankin, A. Ben Altabef, J. Raman Spectrosc. 40 (2009) 2053.
[8] M.E. Defonsi Lestard, M.E. Tuttolomondo, D.A. Wann, H.E. Robertson, D.W.H. Rankin, A. Ben Altabef, J. Chem. Phys. 131 (2009) 214303.
[9] M.J. Frisch, J.A. Pople, J.S. Binkley, J. Chem. Phys. 80 (1984) 3265; M.J. Frisch, G.W. Trucks, H.B. Schlegel, G.E. Scuseria, M.A. Robb, J.R. Cheeseman, J.A. Montgomery Jr., T. Vreven, K.N. Kudin, J.C. Burant, J.M. Millam, S.S. Iyengar, J. Tomasi, V. Barone, B. Mennucci, M. Cossi, G. Scalmani, N. Rega, G.A. Petersson, H. Nakatsuji, M. Hada, M. Ehara, K. Toyota, R. Fukuda, J. Hasegawa, M. Ishida, T. Nakajima, Y. Honda, O. Kitao, H. Nakai, M. Klene, X. Li, J.E. Knox, H.P. Hratchian, J.B. Cross, C. Adamo, J. Jaramillo, R. Gomperts, R.E. Stratmann, O. Yazyev, A.J. Austin, R. Cammi, C. Pomelli, J.W. Ochterski, P.Y. Ayala, K. Morokuma, G.A. Voth, P. Salvador, J.J. Dannenberg, V.G. Zakrzewski, S. Dapprich, A.D. Daniels, M.C. Strain, O. Farkas, D.K. Malick, A.D. Rabuck, K. Raghavachari, J.B. Foresman, J.V. Ortiz, Q. Cui, A.G. Baboul, S. Clifford, J. Cioslowski, B.B. Stefanov, G. Liu, A. Liashenko, P. Piskorz, I. Komaromi, R.L. Martin, D.J. Fox, T. Keith, M.A. Al-Laham, C.Y. Peng, A. Nanayakkara, M. Challacombe, P.M.W. Gill, B. Johnson, W. Chen, M.W. Wong, C. González, J.A. Pople, Gaussian 03, Revision C.02, Gaussian Inc., Wallingford, CT, 2004.
[10] C. Møller, M.S. Plesset, Phys. Rev. 46 (1934) 618.
[11] R. Krishnan, J.S. Binkley, R. Seeger, J.A. Pople, J. Chem. Phys. 72 (1980) 650.
[12] A.D. McLean, G.S. Chandler, J. Chem. Phys. 72 (1980) 5639.
[13] M.J. Frisch, J.A. Pople, J.S. Binkley, J. Chem. Phys. 80 (1984) 3265.
[14] W.J. Hehre, P.V.R. Schleyer, J.A. Pople, Ab initio Molecular Orbital Theory, Wiley, New York, 1986.
[15] A.D. Becke, J. Chem. Phys. 98 (1993) 5648.
[16] C. Lee, W. Yang, R.G. Parr, Phys. Rev. B 37 (1988) 785.
[17] C. Alamo, B. Barone, J. Chem. Phys. 108 (1998) 664.
[18] M.J. Frisch, A.B. Nielsm, A.J. Holder, Gaussview User Manual, Gaussian, Pittsburgh, 2008.

[19] V. Krishnakumar, G. Keresztury, T. Sundius, R. Ramanamy, J. Mol. Struct. 702 (2004) 9.
[20] E.D. Glendening, J.K. Badenhoop, A.D. Reed, J.E. Carpenter, F.F. Weinhold, Theoretical Chemistry Institute, University of Wisconsin, Madison, WI, 1996.
[21] R.F.W. Bader, Atoms in Molecules, A Quantum Theory, Claderon Press, Oxford, 1990.
[22] F. Biegler-Köning, J. Schönnbohn, D. Bayles, J. Comput. Chem. 22 (2001) 545.
[23] Y. Mido, K. Suzuki, N. Komatsu, M. Hashimoto, J. Mol. Struct. 144 (1986) 329.
[24] V.B. Arce, C.O. Della Védova, A.J. Downs, S. Parsons, R.S. Romano, J. Org. Chem. 71 (2006) 3423.
[25] M.E. Defonsi Lestard, R.A. Cobos Picot, M.E. Tuttolomondo, A. Ben Altabef, Vib. Spectrosc. 65 (2013) 124.
[26] D.M. Gil, O.E. Piro, G.A. Echeverria, M.E. Tuttolomondo, A. Ben Altabef, Spectrochim. Acta 116 (2013) 122.
[27] V.B. Arce, C.O. Della Védova, A.J. Downs, S. Parsons, R.M. Romano, J. Org. Chem. 71 (2006) 3423.
[28] M.E. Defonsi Lestard, L.A. Ramos Guerrero, M.E. Tuttolomondo, S.E. Ulic, A. Ben Altabef, Vib. Spectrosc. 55 (2011) 153.
[29] M. Cuaquira Reina, R. Boese, M. Ge, S.E. Ulic, H. Beckers, H. Willner, C.O. Della Védova, J. Phys. Chem. A 112 (2008) 7939.